

Determining the vibrational entropy change in the giant magnetocaloric material $\text{LaFe}_{11.6}\text{Si}_{1.4}$ by nuclear resonant inelastic x-ray scattering

J. Landers,¹ S. Salamon,¹ W. Keune,¹ M. E. Gruner,¹ M. Krautz,² J. Zhao,³ M. Y. Hu,³ T. S. Toellner,³ E. E. Alp,³ O. Gutfleisch,⁴ and H. Wende^{1,*}

¹*Faculty of Physics and Center for Nanointegration Duisburg-Essen (CENIDE), University of Duisburg-Essen, 47057 Duisburg, Germany*

²*IFW Dresden, P.O. Box 270116, 01171 Dresden, Germany*

³*Advanced Photon Source, Argonne National Laboratory, Argonne, Illinois 60439, USA*

⁴*Materials Science, TU Darmstadt, 64287 Darmstadt, Germany*



(Received 29 January 2018; revised manuscript received 16 May 2018; published 18 July 2018)

Magnetocaloric $\text{LaFe}_{13-x}\text{Si}_x$ -based compounds belong to the outstanding materials with potential for efficient solid-state refrigeration. We have performed temperature-dependent ^{57}Fe nuclear resonant inelastic x-ray scattering measurements (in a field $\mu_0 H$ of ~ 0.7 T) of the vibrational (phonon) density of states, VDOS, in $\text{LaFe}_{11.6}\text{Si}_{1.4}$ across the metamagnetic isostructural first-order phase transition at $T_C \sim 192$ K from the low-temperature ferromagnetic (FM) to the high-temperature paramagnetic (PM) phase, in order to determine the change in thermodynamic properties of the Fe lattice at T_C . The experimental results are compared with density-functional-theory-based first-principles calculations using the fixed-spin moment approach. Our combined experimental and theoretical results reveal distinct and abrupt changes in the VDOS of the Fe sublattice across T_C , occurring within a small temperature interval of $\Delta T \leq 12$ K around T_C . This indicates that strong magnetoelastic coupling (at the atomic scale) is present up to T_C , leading to a pronounced lattice softening (phonon redshift) in the PM phase. These changes originate from the itinerant electron magnetism associated with Fe and are correlated with distinct modifications in the Fe-partial electronic density of states $D(E_F)$ at the Fermi energy E_F . From the experimental VDOS we can infer an abrupt increase (jump) in the Fe-partial vibrational entropy ΔS_{vib} of $+6.9 \pm 2.6$ J/(kg K) and in the vibrational specific heat ΔC_{vib} of $+2.7 \pm 1.6$ J/(kg K) upon heating. The increase in magnitude of the vibrational entropy $|\Delta S_{\text{vib}}| = 6.9$ J/(kg K) of the Fe sublattice at T_C upon heating is substantial, if compared with the magnitude of the isothermal entropy change $|\Delta S_{\text{iso}}|$ of 14.2 J/(kg K) in a field change ΔB from 0 to 1 T, as obtained from isothermal magnetization measurements on our sample and using the Maxwell relation. We demonstrate that ΔS_{vib} obtained by nuclear resonant inelastic x-ray scattering is a sizable quantity and contributes directly and cooperatively to the total entropy change ΔS_{iso} at the phase transition of $\text{LaFe}_{13-x}\text{Si}_x$.

DOI: [10.1103/PhysRevB.98.024417](https://doi.org/10.1103/PhysRevB.98.024417)

I. INTRODUCTION

In the struggle to cover the growing demand for air conditioning and refrigeration, solid-state cooling with ferroic materials offers a promising, environment-friendly and energy-efficient alternative to the prevailing gas-compressor scheme (see Ref. [1] and references therein for a recent overview). Here, heat transport is realized, with the help of a ferroelastic, ferroelectric, or ferromagnetic solid being driven through a (preferentially first-order) phase transition under cyclic application and release of an external field. Therefore, the search for advanced magnetocaloric materials is a topical subject of present research activities [2–11]. Among the outstanding materials for solid-state refrigeration are $\text{La}(\text{Fe},\text{Si})_{13-x}$ -based compounds, which exhibit a giant magnetocaloric effect (MCE) near the first-order metamagnetic phase transition at the Curie temperature T_C [12–16]. As excellent cooling materials, $\text{LaFe}_{13-x}\text{Si}_x$ -based systems ($1.0 \leq x \leq 1.6$) are characterized by a large overall isothermal entropy change ΔS_{iso} , combined with a large adiabatic temperature change ΔT_{ad} [12–17]. The

crystallographic structure is equivalent to that of cubic NaZn_{13} (Fm-3c, 112 atoms per unit cell), including two nonequivalent Fe sites, i.e., Fe_I and Fe_{II} on eightfold (8b) and 96-fold (96i) Wyckoff positions, respectively [18,19]. La atoms occupy (8a) sites, whereas Si atoms share the (96i) sites with Fe_{II} atoms [19–21]. Importantly, the first-order magnetostructural transition exhibits an abrupt isostructural atomic volume decrease upon disappearance of ferromagnetism at T_C [22–24], giving rise to a large inverse barocaloric effect [25]. T_C of $\text{LaFe}_{13-x}\text{Si}_x$ is around 200 K (for $x \approx 1.5$) and increases with rising Si content, but simultaneously the transition changes to second order, e.g., at $x > 2.4$, and $|\Delta S_{\text{iso}}|$ significantly decreases [13]. It has been found that T_C can be achieved above room temperature (RT) by interstitial H incorporation [15,26–33]. T_C of the hydrogenated compounds can be precisely tuned near RT by varying Mn substitution [34–39]. This does not change the lattice symmetry and avoids severe degrading of the magnetocaloric properties, making hydrogenated $\text{La}(\text{Fe},\text{Si},\text{Mn})_{13-x}\text{H}_y$ compounds attractive for refrigeration at useful working temperatures.

The total isothermal entropy change ΔS_{iso} is usually partitioned into three components using the relation $\Delta S_{\text{iso}} = \Delta S_{\text{mag}} + \Delta S_{\text{lat}} + \Delta S_{\text{el}}$, i.e., in terms of contributions from

*Corresponding author: heiko.wende@uni-due.de

the magnetic, lattice (or vibrational), and electronic degrees of freedom, respectively [2]. These terms are related to the configurational entropy due to spin disorder, excitation of phonons (lattice vibrations) and changes in the thermal occupation of electronic states, respectively [40]. Mixed interactions, i.e., cross terms in the relation above, are often neglected, although they can be expected for $3d$ metals [2], in particular, since generally applicable approximations for the respective terms are missing. Model calculations [41–43], based on the phenomenological description of the magnetoelastic coupling between spin and lattice degrees of freedom by Bean and Rodbell [44], show that magnetoelastic coupling appears to be responsible for the enhanced MCE in magnetocaloric materials with a first-order phase transition. A similar conclusion was reached by the authors of Ref. [45] using the two-dimensional (2D) Ising model including spin-lattice coupling. Recently, distinct effects of magnetoelastic coupling have been observed (at the atomic scale) in phonon spectra of $\text{La}(\text{Fe},\text{Si})_{13}$ compounds [46]. Exact knowledge of the entangled contributions of the individual terms and cross terms in the relation given above is of paramount importance for the understanding of the thermodynamics of magnetocaloric materials. For instance, when the magnetic and structural transitions are coupled, as in the case of $\text{La}(\text{Fe},\text{Si})_{13}$ -based compounds, one can measure only the total entropy change ΔS_{iso} by magnetization measurements—and not ΔS_{mag} , as the authors of Refs. [3,45] point out. Application of the Maxwell relation $(\partial S/\partial B)_T = (\partial M/\partial T)_B$ to isothermal magnetization measurements for the evaluation of the entropy change under application of an external magnetic field provides ΔS_{iso} , but not ΔS_{mag} alone [3,45]. In the literature, the symbol ΔS_{mag} is therefore often used to indicate that a magnetic measurement was used for determining ΔS_{iso} . Indeed, for $\text{LaFe}_{11.6}\text{Si}_{1.4}$ the total ΔS_{iso} determined calorimetrically agrees well with the value calculated by the Maxwell relation [47]. Also, ΔS_{lat} (or ΔS_{vib}) is difficult to measure separately. Sometimes ΔS_{mag} is determined from the experimental specific heat by subtracting ΔS_{vib} obtained with simplifying assumptions, such as the validity of the Debye model for the vibrational (phonon) density of states [48], which is only a very rough approximation [49] and may thus lead to a wrong decomposition.

There is a debate in the literature on the sign of ΔS_{lat} (or ΔS_{vib}), i.e., whether ΔS_{vib} contributes cooperatively or destructively to the total entropy change ΔS_{iso} at the transition. In our previous work [46] we have demonstrated experimentally by ^{57}Fe nuclear resonant inelastic x-ray scattering (NRIXS) combined with density-functional-theory (DFT) based computations (including spin-resolved electronic band-structure effects) that distinct changes in the phonon spectra and a significant increase in ΔS_{vib} (>0) occur in the Fe subsystem of the $\text{LaFe}_{11.6}\text{Si}_{1.4}$ compound near T_C upon heating from the ferromagnetic (FM) to the paramagnetic (PM) state in zero applied magnetic field [46]. Furthermore, ΔS_{vib} was found to be of sizable magnitude and to contribute *cooperatively* with the electronic and magnetic entropy changes to the magnetocaloric effect [46]. This contradicts the earlier work by Jia *et al.* [50], who estimated changes in magnetic, lattice, and electronic entropies in $\text{LaFe}_{13-x}\text{Si}_x$ based on general thermodynamic theory and a mean-field theory analysis. These authors found that ΔS_{el} is negligibly small and that

the magnetic entropy change ΔS_{mag} is dominant, while the lattice entropy change ΔS_{lat} (here arising from the change of lattice vibrations and elastic energy at T_C) is comparably large and *cancels out* most of the magnetic contribution [50]. Simulations [42] of $\text{La}(\text{Fe},\text{Si})_{13}$ -based alloys as a system of localized spins including magnetoelastic coupling based on the Bean-Rodbell model yield a very good description of the empirical data, suggesting that the entropy change at the transition shall be searched in the spin contribution, while lattice entropy plays only a *minor* and *counteracting* role. Based on their analysis, these authors [42] conclude on a lattice entropy *decrease* ($\Delta S_{\text{lat}} < 0$) at the FM-PM magnetic transition, accompanied by the lattice contraction at T_C upon heating [30]. The conclusions in Ref. [42] contradict the first-principles prediction and NRIXS results (see also the last paragraph of Sec. III B on p. 11). However, in contrast to the *ab initio* approach in Ref. [46], the phenomenological descriptions do not take into account the distinct changes in the electronic structure at T_C , which accompany the itinerant metamagnetic transition and thus also affect the magnetic subsystem in a peculiar way. In view of this discussion, the contribution from the lattice to the MCE presents an interesting basic question [51].

From Ref. [46], only data corresponding to different temperatures were available to corroborate our view, which were not directly located at T_C . In this work we determine the change in the Fe-partial vibrational (lattice) entropy ΔS_{lat} of the compound $\text{LaFe}_{11.6}\text{Si}_{1.4}$ across its magnetostructural phase transition using temperature-dependent ^{57}Fe NRIXS. NRIXS is an atomistic method, being intrinsically sensitive to lattice dynamics [52] and providing the vibrational (phonon) density of states [VDOS, $g(E)$] with a minimum of modeling [53] (see also the description of the used PHOENIX computer program in the Supplemental Material [54]). NRIXS is not *directly* sensitive to magnetic degrees of freedom, e.g., spin waves or magnetic fluctuations. In our former work [46], NRIXS has been proven to be a unique method for the rather direct determination of the VDOS of the Fe sublattice in $\text{LaFe}_{11.6}\text{Si}_{1.4}$. We could demonstrate experimentally by NRIXS and theoretically by DFT-based computations [46] that distinct high-frequency lattice-vibrational (phonon) modes exist in the low-temperature ferromagnetic (FM) state of this cubic material due to magnetoelastic coupling, whereas temperature-induced magnetic disorder causes these phonon modes to disappear in the high-temperature paramagnetic (PM) state above T_C . Upon heating across T_C , this leads to a significant *increase* of the vibrational entropy, ΔS_{vib} , associated with the Fe subsystem.

The present study supports and extends our previous findings [46], and, moreover, precisely quantifies ΔS_{vib} of the Fe subsystem. Our present work discovers that the change ΔS_{vib} occurs in a steplike fashion (“jump”) in a small temperature interval near T_C . The T dependence of the vibrational entropy $S_{\text{vib}}(T)$ is found to be qualitatively similar to the behavior of the total entropy $S_{\text{iso}}(T)$ near T_C , as observed earlier by specific-heat measurements [12], and both quantities are characterized by a jump $\Delta S > 0$ near T_C . Furthermore, a similar jumplike increase at T_C is observed here in the T dependence of the Fe-partial vibrational specific heat $C_{\text{vib}}(T)$ upon heating across T_C . Anomalies at T_C are observed also in other vibrational thermodynamic properties. With the new thermodynamic data

in combination with the fine resolution of data points around the phase transition, our present work supports and significantly extends the results obtained in Ref. [46]. Moreover, the direct comparison with density functional theory calculations employing the fixed spin moment (FSM) method [55–58], which we found to be in good agreement with our experimental data, allows us to distinguish between the effect of spin disorder and longitudinal quenching of the moments on the vibrational properties at T_C .

II. METHODOLOGY

For the measurements, we used a powder sample ($\leq 100 \mu\text{m}$ in grain size) with nominal composition $\text{LaFe}_{11.6}\text{Si}_{1.4}$ and with Fe enriched to 10% in the isotope ^{57}Fe . Details of the sample preparation and sample characterization are described in Refs. [16,37,46]. The ingot, produced by arc-melting in pure Ar atmosphere, was annealed at 1323 K for 7 days in an Ar-filled quartz tube followed by quenching in water. The powder was made by crushing the same material (annealed and quenched ingot) as studied in our former work [46]. The sample was characterized by x-ray diffraction and 14.4-keV Mössbauer backscattering [46], showing that $89 \pm 1\%$ of the Fe atoms in the sample are in the $\text{La}(\text{Fe},\text{Si})_{13}$ phase and only $11 \pm 1\%$ are in the bcc Fe secondary (minority) phase. Magnetic characterization of the powder material was performed using the vibrating sample magnetometer (VSM) option of a Quantum Design PPMS DynaCool with an external field up to 9 T. Field-dependent magnetization measurements, $M(H)$, on the powder sample at 300 K, where only the bcc-Fe impurity phase is ferromagnetic [see Fig. S1 in the Supplemental Material (SM)], allowed determining the bcc-Fe content with higher accuracy than via Mössbauer backscattering, i.e., 10.4 ± 0.1 at. %. Our magnetization-versus-temperature measurements (Fig. S2, see SM), taken at different temperature sweep rates, revealed a first-order FM-to-PM phase transition at $T_C \sim 190$ K for $\mu_0 H = 10$ mT (in agreement with Ref. [12]) and a shift to ~ 191.5 K for $\mu_0 H = 0.7$ T, at the lowest sweep rates, with a small hysteresis ΔT of ~ 1.3 K. In order to determine ΔS_{iso} , isothermal magnetization measurements (measured in steps of 0.5 K) as a function of the applied magnetic field $\mu_0 H$ for various temperatures T close to and above T_C , i.e., in the range from 185 to 204.5 K, were performed, and integration of the Maxwell relation $(\partial S/\partial B)_T = (\partial M/\partial T)_B$ was used, where M is the magnetization and $B = \mu_0 H$ is the magnetic-flux density. Here, we have adopted the numerical procedure described in Refs. [3,59–61]. Integration of the Maxwell relation was done from the starting field $B = 0$ T and the end-field $B = 0.5, 1.0, 1.5, 2.0, 3.0, 4.0, 5.0,$ and 9.0 T, respectively.

^{57}Fe NRIXS [62–64] was performed at the Sector-3 beamline at the Advanced Photon Source, Argonne National Laboratory. The incident x-ray energy was around $E_0 = 14.4125$ keV, being the nuclear resonance energy of the ^{57}Fe nucleus. After passing through a high-resolution crystal monochromator, the x-ray beam had an energy bandwidth of 1 meV [65]. A toroidal mirror was used to collimate the monochromatized beam and redirect it into a downstream station, where a closed-cycle cryostat was used for the experiment. An avalanche photodiode (APD) detector was placed right outside the dome-shaped Be

window of the cryostat to collect NRIXS signals at grazing incidence (at 4°) of the beam relative to the sample surface. Using epoxy resin, the sample powder was affixed onto the surface of a Cu plate that was mounted (together with two permanent magnets) on the Cu cold head of the cryostat. The Fe-specific VDOS was extracted from the NRIXS data using the PHOENIX program [66,67] (a brief description of the PHOENIX program is presented in the SM). The inelastic nuclear resonant absorption of 14.4125 keV x-rays is selective to the Fe partial vibrational density of states, $g(E)$, rather directly with a minimum of modeling [53,66–68]. The present NRIXS was carried out in the temperature range between 176 and 301 K, with the sample exposed to an external field $\mu_0 H$ of ~ 0.7 T, produced by two small permanent magnets surrounding the sample. This small field was applied in order to suppress possible spin fluctuations in the sample near the Curie temperature T_C , which could possibly smear the transition. The nominal temperature was measured by a thermocouple fixed to the cold head of the cryostat and was controlled to within 0.02 K. The actual $\text{LaFe}_{11.6}\text{Si}_{1.4}$ -sample temperature was determined from the rule of “detailed-balance,” which is intrinsic to NRIXS spectra and uses the fact that in the measured phonon sidebands (see Fig. S3 in the SM) the ratio of the contribution from phonon annihilation, $S(-E)$, and phonon creation, $S(+E)$, at phonon energy $|E|$ is equal to the Boltzmann factor, $\exp(-|E|/k_B T)$ [67]. An average offset between detailed balance sample temperature (T_{DB}) extracted from NRIXS data and nominal cold head temperature (T_{nom}) was determined to be about 4 K in the relevant temperature range of 180–200 K studied in detail, wherefore all temperatures T given here for NRIXS data are corrected by this value, i.e., $T = T_{\text{nom}} + 4$ K for NRIXS. The thermodynamic quantities $S_{\text{vib}}(T)$ and $C_{\text{vib}}(T)$ at a certain temperature T were calculated from the VDOS, $g(E)$, measured at that temperature, and using the textbook thermodynamic relations [69–71] for $S_{\text{vib}}(T)$ and $C_{\text{vib}}(T)$, respectively, as given in Eqs. (1) and (2), respectively, of the present Supplemental Material. The measured VDOS was corrected for the 10.4-at. % bcc-Fe secondary phase by a subtraction and renormalization procedure (as described in the SM of Ref. [46]) in order to obtain the VDOS of the pure $\text{LaFe}_{11.6}\text{Si}_{1.4}$ phase (see also Fig. S4 in the SM).

The computations were performed using the VASP package [72,73] in the framework of density functional theory (DFT) using the generalized gradient approximation [74]. We represented the 112-atom unit cell by a 28-atom primitive cell with fcc basis and introduced three Si atoms on the (96i) sites, i.e., $x = 1.5$ Si per formula unit (f.u.), such that the space group is minimally reduced to rhombohedral ($R3$) with still 12 inequivalent lattice sites. For the PM phase, we determined a stable collinear spin structure with ten inverted Fe moments, which has a total spin magnetization of $3.75\mu_B/\text{f.u.}$ compared to $24.5\mu_B/\text{f.u.}$ for the FM phase. An average spin moment of $1.7\mu_B/\text{Fe}$ was obtained for PM as compared to $2.2\mu_B/\text{Fe}$ for FM. We optimized ionic positions and volume before the dynamical matrix was constructed with Alfé’s PHON code [75] based on the Hellman-Feynman forces. This yields the VDOS, $g(E)$, from which we obtain thermodynamic quantities such as the vibrational entropy, S_{vib} , the vibrational specific heat at constant volume, C_{vib} , and their temperature dependence [69–71]. Further details are reported in Refs. [46,76].

TABLE I. Data obtained from Fig. 1(b), ΔB = change of applied field (relative to $B = 0$ T), $\Delta S_{\text{iso}}(\text{max})$ = maximum entropy change, and T_{max} = temperature at $\Delta S_{\text{iso}}(\text{max})$.

ΔB (T)	$\Delta S_{\text{iso}}(\text{max})$ (J mol ⁻¹ K ⁻¹)	$\Delta S_{\text{iso}}(\text{max})$ (J kg ⁻¹ K ⁻¹)	T_{max} (K)
0.5	-5.3	-6.4	188.1
1.0	-11.7	-14.2	189.2
1.5	-14.8	-17.9	190.7
2.0	-16.0	-19.4	191.7

In order to distinguish between the effect of spin disorder and longitudinal quenching of the moments, we employed the fixed spin moment (FSM) method [55–58] to constrain the total magnetization M of the entire 28-atom cell within the FM configuration. The FSM method has become a standard technique for analyzing the presence of magnetically distinct states in the system as the constraint allows us to stabilize a specific magnetic configuration. For instance, it was successfully applied to resolve the interplay of high-spin and low-spin states in fcc-Fe and Invar alloys [58,77–80]. The FSM approach has been also used to understand itinerant electron metamagnetism in La(Fe,Si)₁₃-type compounds from the electronic structure point of view [81–83]. The cell parameters and atomic positions were allowed to adapt freely after the change of the magnetization M of the entire cell. This (artificial) homogeneous ferromagnet with the constrained magnetization $M = 20\mu_B/\text{f.u.}$, denoted by FSM in the following, has reduced magnetic moments of $1.8\mu_B/\text{Fe}$ as the PM, but full ferromagnetic order as the FM state. Further discussion of this state can be found in Ref. [76].

III. RESULTS AND DISCUSSION

A. Isothermal entropy change ΔS_{iso}

Figure 1(a) shows the measured isothermal magnetization (measured in steps of $\Delta T = 0.5$ K) as a function of the external magnetic field $\mu_0 H$ for various temperatures T close to and above T_C , i.e., in the range from 185 to 204.5 K. Typical metamagnetic behavior of La(Fe,Si)₁₃ is observed in Fig. 1(a), in qualitative agreement with results in Ref. [84]. The isothermal entropy change ΔS_{iso} , obtained from the magnetization data of Fig. 1(a) and use of the Maxwell relation, is shown in Fig. 1(b). We obtained peaked $\Delta S_{\text{iso}}(T)$ functions for field changes of $\Delta B = 0.5, 1.0, 1.5,$ and 2.0 T. The results are presented in Table I. As expected, $\Delta S_{\text{iso}}(\text{max})$ (<0) is reduced by applying a magnetic field [12,84]. Our result at $\Delta B = 2$ T [$\Delta S_{\text{iso}}(\text{max}) = -19.4$ J/(kg K)] is in reasonable agreement with the corresponding literature values of -24 J/(kg K) for LaFe_{11.57}Si_{1.43} [12] or about -19 J/(kg K) for LaFe_{11.6}Si_{1.4} [16]. Here, we would like to mention that $\Delta S_{\text{iso}}(\text{max})$ depends on the annealing temperature during sample processing [16]. One can observe in Fig. 1(b) that a plateaulike behavior of $\Delta S_{\text{iso}}(T)$ develops for B larger than 2 T, in agreement with Ref. [12].

B. Nuclear resonant inelastic x-ray scattering (NRIXS) and DFT-based computations

Figure 2 exhibits typical Fe-partial VDOS of the LaFe_{11.6}Si_{1.4} powder sample obtained by ⁵⁷Fe NRIXS in a field

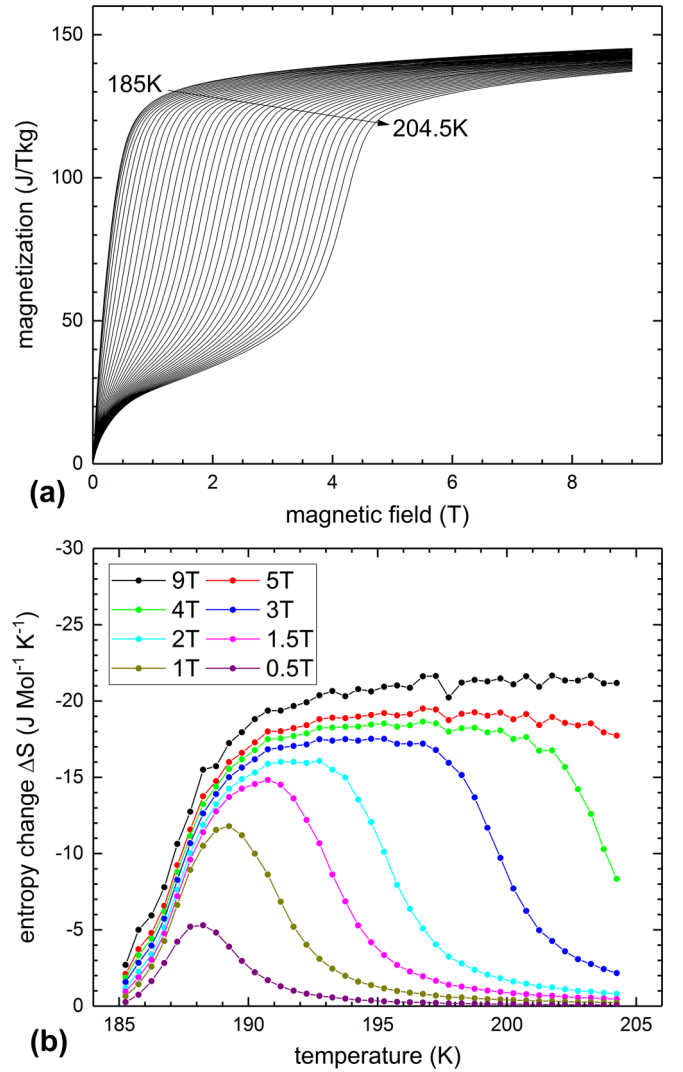


FIG. 1. (a) Isothermal magnetization vs applied field of LaFe_{11.6}Si_{1.4} powder (enriched to 10% in ⁵⁷Fe) measured by vibrating sample magnetometry (VSM) in the temperature interval from 185 to 204.5 K in temperature steps of 0.5 K upon increasing temperature and increasing field $\mu_0 H$. In order to exclude sample-history magnetic effects, before each isothermal $M(H)$ measurement, the sample was heated in zero field to 300 K, i.e., to a temperature far above the zero-field Curie temperature of $T_C = 188$ K. This was followed by careful zero-field cooling to the measurement temperature T to avoid a temperature overshoot of the sample, and the subsequent $M(H)$ measurement at the starting field $B = 0$ T up to the maximum end field $B = 9$ T. (b) Entropy change ΔS_{iso} , obtained from the data in Fig. 1(a) using integration of the Maxwell relation $(\partial S/\partial B)_T = (\partial M/\partial T)_B$ between the starting field $B = 0$ T and the end field $B = 0.5, 1.0, 1.5, 2.0, 3.0, 4.0, 5.0,$ and 9.0 T, respectively.

of ~ 0.7 T across the metamagnetic transition temperature T_C of ~ 192 K upon decreasing temperature. (The corresponding NRIXS raw data are shown in Fig. S3 of the SM). In Fig. 2, the VDOS at 180 and 188 K [in the ferromagnetic (FM) state] show clear differences as compared to the VDOS in the paramagnetic (PM) state at 200 and 301 K. In particular, striking differences in the VDOS below and above T_C can be observed by the disappearance of the distinct high-energy phonon peak near 27

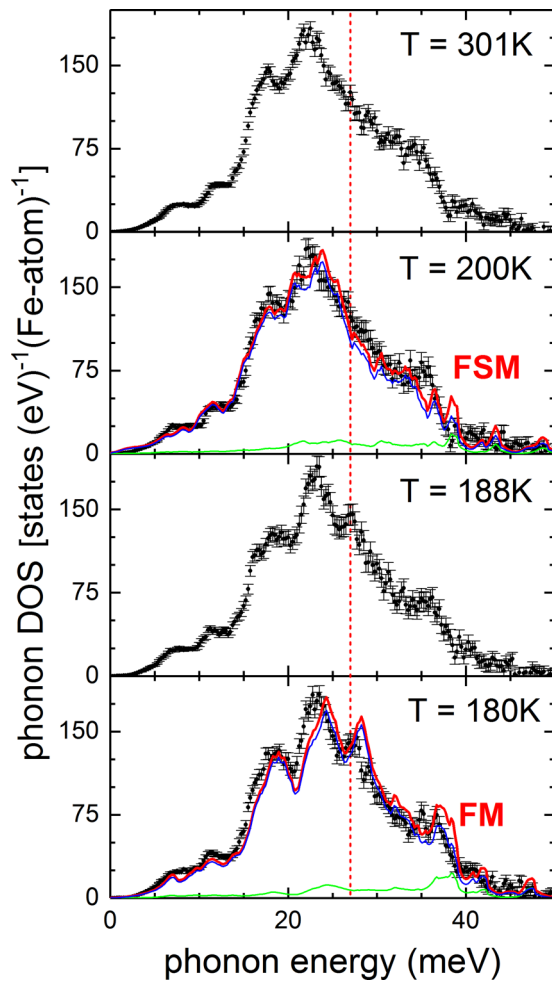


FIG. 2. Typical Fe-partial vibrational (or phonon) density of states, VDOS, of $\text{LaFe}_{11.6}\text{Si}_{1.4}$ powder (10% enriched in ^{57}Fe) obtained by ^{57}Fe NRIXS in a field of $\mu_0 H \sim 0.7$ T close to the metamagnetic transition temperature of ~ 192 K at $\mu_0 H \sim 0.7$ T (black circles with error bars). Four representative VDOS are shown: Two VDOS above T_C (measured at 200 and 301 K, respectively) and two VDOS below T_C (measured at 188 and 180 K, respectively). The NRIXS spectra were taken upon decreasing temperature. The vertical dashed red line marks the phonon energy of ~ 27 meV, where the phonon mode, prominent in the ferromagnetic (FM) state ($T < T_C$), abruptly disappears in the paramagnetic (PM) state ($T > T_C$). Red curves: DFT-calculated Fe-partial VDOS for the FM state and the FSM state, respectively, in $\text{LaFe}_{11.5}\text{Si}_{1.5}$. Thick lines: Total Fe-partial VDOS. The thin lines show the respective computed contributions from the (96*i*) Fe_{II} (blue) and (8*b*) Fe_{I} sites (green), respectively. The experimental data at 180 K exhibit a redshift relative to the computed VDOS of the FM state. The redshift is less pronounced between the experimental data at 200 K (in the PM state) and the computed VDOS of the FSM state. The calculated VDOS of the FM state and the FSM state was taken from Refs. [46,76], respectively. The experimental data show the bcc-Fe (impurity-phase-) corrected VDOS of pure $\text{LaFe}_{11.6}\text{Si}_{1.4}$.

meV (vertical red line in Fig. 2) in the paramagnetic state. The existence of the prominent 27-meV phonon peak in the ferromagnetic state is a direct manifestation of the effect of magnetoelastic (or spin-phonon) coupling of Fe magnetic moments in

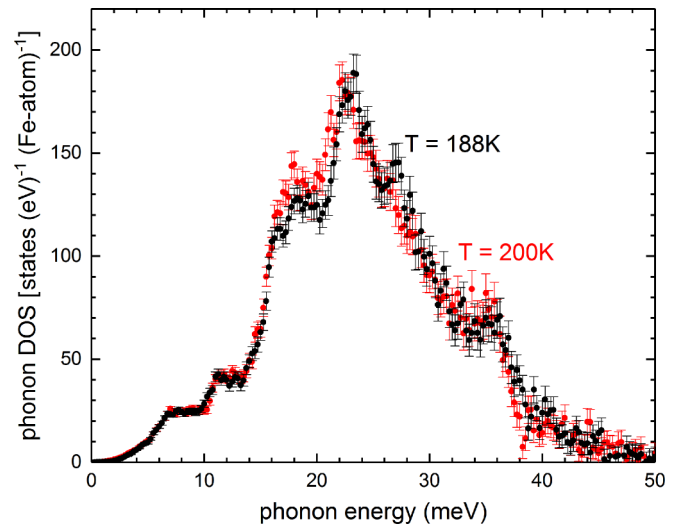


FIG. 3. Fe-partial vibrational (or phonon) density of states, VDOS, of $\text{LaFe}_{11.6}\text{Si}_{1.4}$ powder (10% enriched in ^{57}Fe) obtained by ^{57}Fe NRIXS in a field $\mu_0 H \sim 0.7$ T close to the metamagnetic transition temperature of ~ 192 K at 0.7 T. One VDOS was taken at $T = 188$ K ($< T_C$, black dots), and the other VDOS was taken at $T = 200$ K ($> T_C$, red dots). The NRIXS spectra were taken upon decreasing temperature. The prominent high-energy phonon peak at 188 K is quenched abruptly within $\Delta T = 12$ K by going to the paramagnetic state (at 200 K). This observation provides atomistic evidence of strong magnetoelastic coupling in the FM state. Furthermore, a clear average shift $\Delta E/E$ of -1.5% of the VDOS at 200 K relative to the VDOS at 188 K is observed (redshift), indicating overall phonon softening within $\Delta T \sim 12$ K by heating across the magnetostructural transition. For example, this corresponds to a shift ΔE of -0.54 meV (-0.33 meV) for the high-energy phonons at 36 meV (22 meV). The experimental data show the bcc-Fe (impurity phase) corrected VDOS of pure $\text{LaFe}_{11.6}\text{Si}_{1.4}$.

the FM state. With the onset of magnetic disorder above T_C , the phonon spectrum is drastically modified. Our result in Fig. 2 demonstrates that the change in the VDOS occurs between 188 and 200 K, i.e., within a small temperature interval of at most $\Delta T = 12$ K around T_C . This is more clearly shown in Fig. 3, where the two VDOS at 188 K ($T < T_C$) and 200 K ($T > T_C$) are directly compared. Besides the disappearance of the ~ 27 -meV phonon mode in the PM state (at 200 K), a striking overall shift $\Delta E/E$ (of -1.5%) in the VDOS towards lower energy (redshift, $\Delta E/E < 0$) is observed in the PM state relative to the FM state (188 K), i.e., within only 12 K across T_C . Our earlier work [46] already delivered strong indications for the presence of this redshift, but only with the fine temperature resolution of our current measurements is a quantitative verification possible within a narrow temperature interval across T_C . Keeping in mind that at the magnetic order-disorder transition only the volume decreases considerably, while lattice symmetry is conserved, the observed redshift is highly counterintuitive. One might assume that the change in magnetic order has only a minor effect on the interatomic forces, which apparently stabilize the same cubic structure. It is then natural to account for the decrease in volume in terms of the classical Grüneisen theory [85]. This is the usual procedure in simulations using localized

spin models, e.g., in terms of a generalized Bean-Rodbell model. In such a case one would expect a blueshift ($\Delta E/E > 0$) in phonon energy E (and not a redshift) according to the Grüneisen relation $\Delta E/E = -\gamma (\Delta V/V)$, where $\gamma > 0$ is the—usually positive—average-mode Grüneisen constant, and $\Delta V/V < 0$ is the relative atomic volume contraction upon magnetic disorder. The verification of the redshift within this small temperature proves that not only the 27-meV peak but rather the entire VDOS is renormalized by the change in magnetic order, pointing out considerable modifications of the interatomic potentials around T_C . Thus, in a strict sense, the simplified Grüneisen picture is not applicable here, since the volume-dependent changes in the VDOS are not described by an average γ , which is most easily seen from the disappearance of the 27-meV mode at the transition. Nevertheless, defining an effective average Grüneisen parameter can still be useful to compare the thermodynamic behavior of different materials.

Generally, the Grüneisen parameter γ will take values between 1 and 3 for most solid materials [85,86]. For $\text{LaFe}_{11.6}\text{Si}_{1.4}$ at the FM-to-PM transition, we can calculate γ using $\Delta V/V = -1.45\%$ from Fig. 3 in Ref. [50] and from our experimental value $\Delta E/E = -1.5\%$ for the overall VDOS redshift from NRIXS. Applying the Grüneisen relation $\Delta E/E = -\gamma(\Delta V/V)$, we obtain $\gamma = -1$, i.e., a negative (effective) Grüneisen parameter at the first-order phase transition. Furthermore, the Grüneisen parameter is related to the linear thermal-expansion coefficient α by the relation $\gamma = \alpha(3B/C_V)$, where $B > 0$ is the isothermal bulk modulus and $C_V > 0$ is the specific heat at constant volume [87]. Keeping in mind that the measured thermal-expansion coefficient α of $\text{LaFe}_{13-x}\text{Si}_x$ (e.g., with $x = 1.56$) was reported to show a strongly peaked large *negative* value at the first-order FM-to-PM transition [88], this suggests (using the above equation) a *negative* Grüneisen parameter at the phase transition. Another example for a negative γ value is the first-order antiferromagnetic-to-paramagnetic transition at the Néel temperature $T_N = 311$ K in Cr. For the latter, a large negative value of γ at T_N was reported [89]. It is worth mentioning that negative values for the acoustic-mode Grüneisen parameter have also been observed in Fe-Pt Invar alloys, again accounting for the negative thermal expansion $\alpha < 0$ in the temperature range between about 260 K and the Curie temperature T_C of these alloys [90]. In some nonferromagnetic compounds it was experimentally observed via inelastic neutron scattering that unusual phonon softening on lattice contraction, which corresponds to a large negative Grüneisen parameter, is able to account for the observed large negative thermal expansion in cubic ZrW_2O_8 [91] and similar materials [92]. Summarizing, we can say that (in addition to our present observation on $\text{LaFe}_{11.6}\text{Si}_{1.4}$) negative Grüneisen parameters are observed in certain materials characterized by unusual negative thermal expansion, i.e., contraction of the lattice with rising temperature.

Our experimental findings described above are in quantitative agreement with our DFT-based computational results, as presented in Fig. 2, where we compare the Fe-partial VDOS computed for the FSM configuration (red line) with the Fe-partial VDOS measured in the PM state at 200 K, i.e., only ~ 8 K above the magnetic transition. We observe overall excellent agreement between the calculated (FSM) and ex-

perimental (PM) VDOS; even fine details of the experimental VDOS are represented in the computed VDOS. This includes, in particular, the absence of the phonon peak at ~ 27 meV and the appearance of the anomalous redshift, which, however, is slightly overestimated by the FSM calculation. The overall small redshift of the experimental VDOS at 180 K relative to the DFT-computed VDOS of the FM state might be attributed to the effect of thermal expansion on the VDOS in the sample at 180 K, in combination with the indirect effect on the VDOS of a reduction of the local Fe moments arising from thermal magnetic excitations, as compared to the DFT-calculated VDOS, which represents $T = 0$ K. As already pointed out in our previous work [46], the qualitative changes in the VDOS are a microscopic manifestation of the magnetoelastic coupling, which has a strong impact on the Fe subsystem at the magnetic order-disorder transition. Due to the itinerant electron metamagnetism of Fe, not only the directional order but also the magnitude of the Fe moments change at T_C [76,81,82,88]. The FSM state represents an ordered system with artificially reduced Fe moments, as appropriate for the PM state. The excellent agreement of the FSM VDOS with the experimental NRIXS data in the PM phase proves that in the first line not the change in order but the change in magnitude of the magnetic moments is responsible for the strong magnetoelastic effects. Therefore, we can conclude that the magnetoelastic coupling is closely related to the itinerant nature of the Fe moments. This rather reminds one of a moment-volume coupling which is typical for Invar-type systems (e.g., Ref. [93]), rather than of the interaction of lattice vibrations with the excitations of localized spins (magnon-phonon coupling).

As $\text{LaFe}_{13-x}\text{Si}_x$ has two inequivalent Fe sites, one may inquire for the site-specific contributions. However, the difference in hyperfine interactions that is sensed by the nuclei of the nonequivalent Fe_I and Fe_{II} sites (of the order of 100 neV), which is visible via Mössbauer spectroscopy (e.g., in Refs. [46,94]), could not be resolved in our NRIXS measurements, since the incoming monochromatized 14.4-keV beam has an energy resolution of ≈ 1 meV and nuclei of both sites are excited. However, as demonstrated by Seto *et al.* the discrimination of different Fe sites may be possible, in particular if these are connected to different oxidation states of Fe [95]. In the present case of $\text{La}(\text{Fe},\text{Si})_{13}$, where the two nonequivalent Fe sites exhibit extreme site occupancies of 1:12 and, furthermore, are in the metallic electronic state, the discrimination of the two Fe sites via the method by Seto *et al.* appears to be a great challenge. As the ratio of crystallographic abundance of ($8b$) to ($96i$) sites is 1:12, the measured Fe VDOS is typical for the dominant Fe_{II} species. This is confirmed by the calculated VDOS, which can be partitioned into the contributions from all inequivalent sites. According to their different crystallographic environment, the VDOS associated with the Fe_I atoms has indeed a qualitatively different shape in both phases. Compared to the Fe_{II} , weight is shifted to higher energies (30 meV), while the above-mentioned 27-meV peak is missing for Fe_I in both phases. Still, the comparison of the FM and FSM VDOS reveals that also for the Fe_I atoms moment-volume coupling induces distinct changes in the prominent features at T_C .

A further important result of our present study is shown in Fig. 4, where we exhibit the temperature dependence of

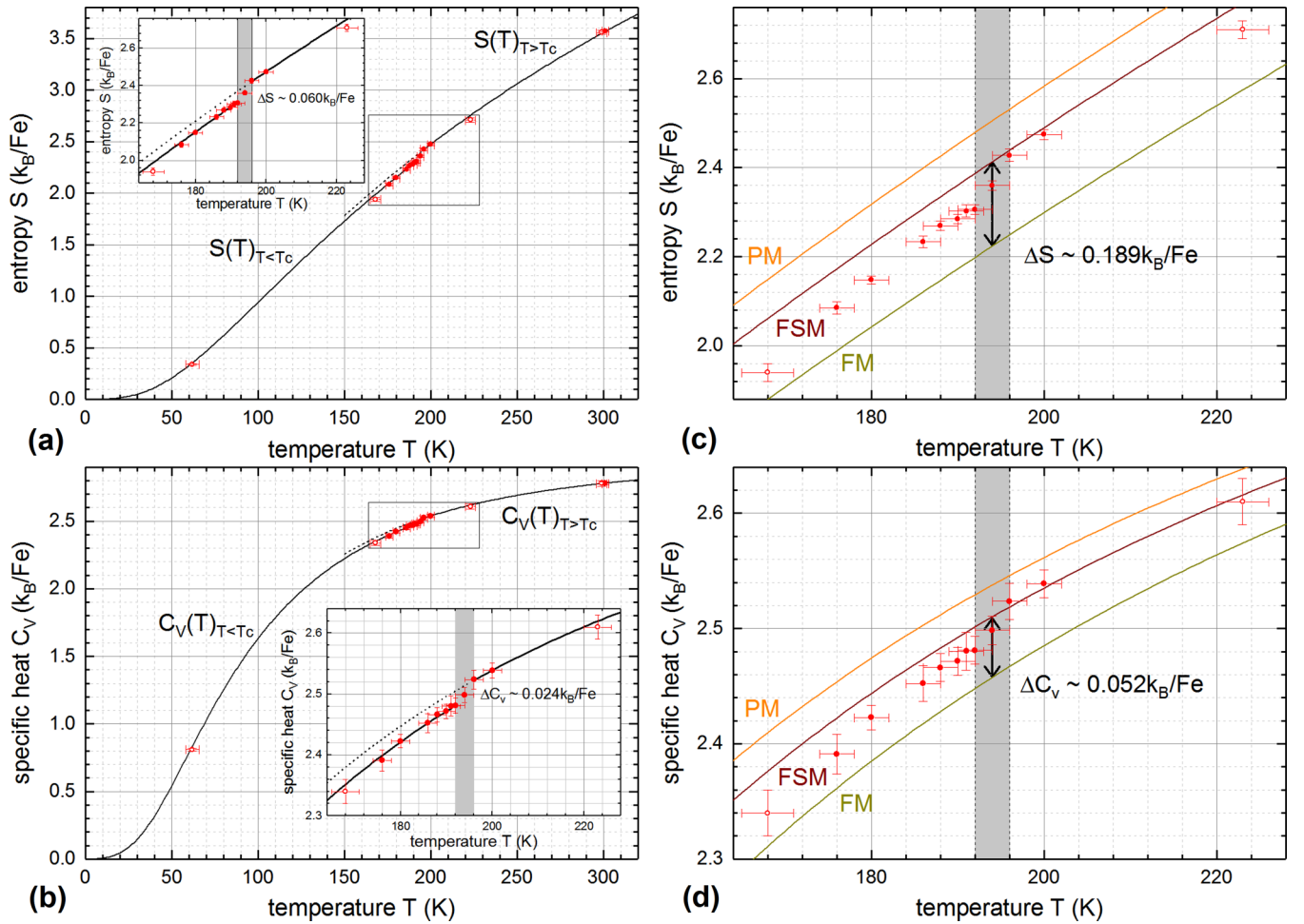


FIG. 4. Temperature dependence of the experimental (a) and DFT-computed (c) vibrational entropy $S_{\text{vib}}(T)$ and of the experimental (b) and DFT-computed (d) vibrational specific heat $C_{\text{vib}}(T)$ at constant volume, of the Fe sublattice. The experimental data (red circles) were taken on $\text{LaFe}_{11.6}\text{Si}_{1.4}$ powder in a field $\mu_0 H$ of ~ 0.7 T upon decreasing measurement temperatures. (The four red open circles are data measured independently in zero external field and are taken from Ref. [46]). The two lines drawn in (a) and (b) correspond to the extrapolated T dependence of $S_{\text{vib}}(T)$ and $C_{\text{vib}}(T)$, respectively, calculated from Eqs. (1) and (2), as given in the SM, from experimental VDOS curves in the paramagnetic ($T > T_c$, upper line) and the ferromagnetic region ($T < T_c$, lower line), respectively. The insets in (a) and (b) show a magnification of the region close to the magnetostructural transition. From the insets, the transition temperature (indicated by the vertical gray bar) is estimated to $T_c \sim 192$ – 196 K. The DFT-based computed results in (c) and (d) exhibit $S_{\text{vib}}(T)$ and $C_{\text{vib}}(T)$ at constant volume, respectively, for $\text{LaFe}_{11.5}\text{Si}_{1.5}$ in the vicinity of the magnetostructural transition at ~ 192 K. The lines drawn in (c) and (d) result from the DFT-calculated Fe-partial VDOS for the FM state (lower olive line), the FSM state (middle magenta line) and the PM state (upper orange line), and using the thermodynamic relations [69–71] for $S_{\text{vib}}(T)$ and $C_{\text{vib}}(T)$, respectively. The red full dots in (c) and (d) represent the experimental data for comparison, and the vertical black arrows indicate the computed vibrational entropy change ΔS_{vib} in (c) and the computed vibrational specific-heat change at constant volume ΔC_{vib} in (d), at the transition. [The computed results for $S_{\text{vib}}(T)$ and $C_{\text{vib}}(T)$ that extend over a larger temperature range are shown in Fig. S5 of the SM]. Further details are described in the text.

the experimental [Fig. 4(a)] and DFT-computed [Fig. 4(c)] vibrational entropy $S_{\text{vib}}(T)$ and of the experimental [Fig. 4(b)] and DFT-computed [Fig. 4(d)] vibrational specific heat $C_{\text{vib}}(T)$ at constant volume for the Fe sublattice in $\text{La}(\text{Fe}, \text{Si})_{13}$. We discuss the experimental results first. The bcc-Fe impurity-phase corrected VDOS, $g(E)$, of pure $\text{LaFe}_{11.6}\text{Si}_{1.4}$ was used for the calculation of the thermodynamic quantities. The experimental data (red circles with error bars) were taken with decreasing measurement temperature. The data points for $S_{\text{vib}}(T)$ in Fig. 4(a) and for $C_{\text{vib}}(T)$ in Fig. 4(b) were calculated from the VDOS, $g(E)$, measured at specific temperatures (red symbols), and using thermodynamic relations [69–71] for $S_{\text{vib}}(T)$ and

$C_{\text{vib}}(T)$, respectively, as given in Eqs. (1) and (2), respectively, of the Supplemental Material. The four open circles are data measured independently in zero external field and taken from Ref. [46]. The two lines drawn in Figs. 4(a) or 4(b) were obtained via Eqs. (1) and (2) (see the SM), by calculating the temperature-dependent entropy and specific heat, respectively, from experimental VDOS curves determined either below or above the phase transition (at T_c of about 192 K). One can see that the two fitted curves in Fig. 4(a) describe the data points for the FM and PM region, respectively, very well, independent of in-field (~ 0.7 T) or zero-field measurements. Since Eq. (1) for $S_{\text{vib}}(T)$ (see the SM) is valid for constant volume V ,

the good fit in the wide FM region in Fig. 4(a) implies that $g(E)$ is rather independent of temperature and that thermal lattice expansion is very small (Invar-type behavior) below T_C [22–24,27,88], and, furthermore, that $g(E)$ is independent of the magnetization M in the FM regime. In fact, comparison of $g(E)$ curves measured in zero external field in the FM region at ~ 62 and 164 K, respectively, demonstrates that both $g(E)$ functions are of similar shape and differ only by a tiny redshift (see Figs. S8 and S10 in the Supplemental Material of Ref. [46]). Similar observations were made for $g(E)$ curves obtained at 220 and 299 K in the PM region for $T > T_C$ (see Figs. S8 and S10 in the Supplemental Material of Ref. [46]), where also thermal lattice expansion is rather small [22–24,27,88]. The inset in Fig. 4(a) shows a magnification of the region close to the magnetostructural transition and exhibits a rather abrupt increase (“jump”) (within $\Delta T \leq 12$ K) in S_{vib} by $\Delta S_{\text{vib}} = (+0.060 \pm 0.023)k_B/\text{Fe atom}$ [or $(+6.9 \pm 2.6)$ J/(kg K)] upon heating across the transition. From the inset, the transition temperature (indicated by the vertical gray bar) is estimated to approximately $T_C = 192\text{--}196$ K, in excellent agreement with $T_C = 192$ K (at 0.7 T) obtained from our magnetization measurement (Fig. S2, Supplemental Material).

A comparison of our result for ΔS_{vib} of the Fe subsystem with the total entropy jump ΔS_{iso} [12] observed for $\text{La}(\text{Fe}_{0.88}\text{Si}_{0.12})_{13}$ (being of similar composition as our $\text{LaFe}_{11.6}\text{Si}_{1.4}$ sample) is informative. The T dependence of the total entropy $S_{\text{iso}}(T)$ (Fig. 1 in Ref. [12], obtained via in-field specific-heat measurements) exhibits an estimated jump ΔS_{iso} of about $+18$ J/(kg K) near T_C at an applied field $\mu_0 H = 1$ T, i.e., at an only slightly larger applied field as in our present study (0.7 T). At a field of 5 T the jump ΔS_{iso} is equal to $+24$ J/(kg K) [12]. This comparison reveals two important facts: (i) both the vibrational entropy $S_{\text{vib}}(T)$ and the total entropy $S_{\text{iso}}(T)$ increase rather abruptly and cooperatively at the magnetostructural transition upon heating from the FM to the PM state (i.e., $\Delta S_{\text{vib}} > 0$ and $\Delta S_{\text{iso}} > 0$), and (ii) although the magnitude of our value of $\Delta S_{\text{vib}} = 6.9$ J/(kg K) is smaller than the magnitude of $\Delta S_{\text{iso}} \sim 18$ J/(kg K) at $\mu_0 H = 1$ T or 24 J/(kg K) at 5 T in Ref. [12], the lattice contributes cooperatively with $\sim 38\text{--}29\%$ to the total entropy at T_C and, therefore, plays an important role for the magnetocaloric effect. This contradicts the claims in Refs. [42,43,50] on the counteracting role of ΔS_{lat} , as mentioned in our Introduction. It is also interesting to notice that the magnitude of the Fe-partial change in vibrational entropy, $|\Delta S_{\text{vib}}| = 6.9$ J/(kg K), is relatively large and amounts to $\sim 49\%$ of the magnetic entropy change $|\Delta S_{\text{tot}}| = 14.2$ J/(kg K) at $\mu_0 H = 1$ T [Fig. 1(b)] obtained for our sample using the Maxwell relation. Also this comparison proves that $|\Delta S_{\text{vib}}|$ is a sizable quantity for the description of the magnetocaloric effect in $\text{La}(\text{Fe},\text{Si})_{13}$ compounds.

The above description for $\Delta S_{\text{vib}}(T)$ in Fig. 4(a) is valid also for $\Delta C_{\text{vib}}(T)$ in Fig. 4(b), except that $C_{\text{vib}}(T)$ was calculated from $g(E)$ using the corresponding thermodynamic relation, Eq. (2) (see the Supplemental Material). The inset in Fig. 4(b) shows a magnification of the region close to the magnetostructural transition and exhibits a rather abrupt increase (within $\Delta T \leq 12$ K) in C_{vib} by $\Delta C_{\text{vib}} = (+0.024 \pm 0.013)k_B/\text{Fe atom}$ [or $(+2.7 \pm 1.6)$ J/(kg K)] for the Fe subsystem upon heating across the transition. The transition temperature $T_C \sim$

$192\text{--}196$ K, estimated from Figs. 4(a) and 4(b), is in excellent agreement with $T_C \sim 192$ K (also in a field of 0.7 T) obtained from our magnetization measurements, as shown in Fig. S2 (Supplemental Material). The two fitted curves in Fig. 4(b) describe the data points for the FM and PM region, respectively, rather well. Since Eq. (2) (see the SM) for $C_{\text{vib}}(T)$ is valid for constant volume V , the good fits in the FM and PM region, respectively, in Fig. 4(b) imply that $g(E)$ is rather independent of temperature in the selected temperature interval below and above T_C , respectively, and that, consequently, thermal lattice expansion is small in the chosen temperature regions below and above T_C [22–24,27,88].

In Fig. 4(c) we compare, for the Fe subsystem, the temperature dependence of the DFT-computed vibrational entropy $S_{\text{vib}}(T)$ at constant volume for the FM, PM, and FSM states with the experimental result. Figure 4(c) exhibits a zoom of the region around the phase transition at $T_C \sim 192$ K. The theoretical results, represented by the drawn lines, qualitatively confirm the experimental observations (full red circles with error bars). In the FM state, i.e., below T_C , the DFT calculated result (lowest line, olive) follows the experimental data rather closely, whereas in the PM state, i.e., above T_C , the calculated result (upper line, orange) deviates from the experimental data. However, much better agreement with the experimental data in the PM region can be noticed for the FSM result (middle line, magenta). In qualitative agreement with the experimental data, the computed values of $S_{\text{vib}}(T_C)$ for PM and FSM states are found to be larger than the computed value of $S_{\text{vib}}(T_C)$ for the FM phase. Thus, in agreement with the experiment, we notice an increase of the Fe-partial computed vibrational entropy at the FM-to-PM transition. From Fig. 4(c), we can estimate a computed vibrational entropy change ΔS_{vib} (theory) of about $+0.189k_B/\text{Fe}$ [or about $+22$ J/(kg K)] between the FSM and the FM state of the Fe subsystem. This is about 3.2 times larger than the experimental Fe-partial entropy jump of $+0.060k_B/\text{Fe}$ [or $+6.9$ J/(kg K)] that occurs at the FM-to-PM transition [Fig. 4(a)]. Comparison with the experimental data points shows that the calculations of the FM state underestimate, and of the PM and FSM states overestimate, the experimental data directly at the transition, while they reproduce the experiments at low temperatures and RT quite well [see Fig. S5 in the SM, where $S(T)$ is shown in a wide temperature range]. We are therefore inclined to ascribe the deviations to the presence of magnetic fluctuations in the FM phase, which increase S_{vib} due to the magnetoelastic coupling mechanism described above. In turn, close to T_C , ferromagnetic clusters may already be present in the undercooled PM phase, leading to a smaller S_{vib} than for a perfect paramagnet. This interpretation is supported by the experimental observation that in typical samples thermal expansion directly above T_C remains negative at first until T reaches 220 K for $\text{LaFe}_{11.7}\text{Si}_{1.3}$ [24], suggesting that the fraction of the PM phase still increases with temperature. We would like to emphasize that the change $\Delta S_{\text{vib}}(T_C)$ for both theory and experiment is of sizable magnitude and is comparable to the measured value of the total entropy change ΔS_{iso} . For example, ΔS_{iso} is found to be about $+18$ J/(kg K) near T_C in a field of $\mu_0 H = 1$ T for $\text{LaFe}_{11.6}\text{Si}_{1.4}$ [12].

Similar observations as for the entropy can be made for the T dependence of the computed vibrational specific heat $C_{\text{vib}}(T)$ at constant volume of the Fe subsystem, as shown

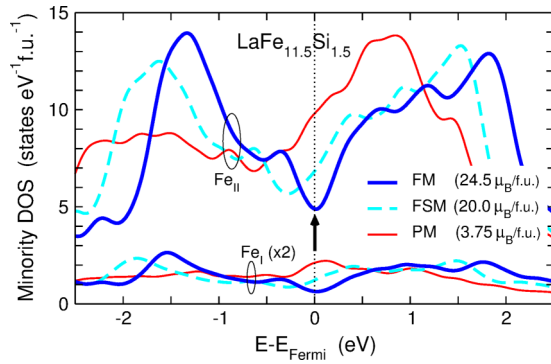


FIG. 5. DFT-computed electronic density of states, $D(E)$, for minority d electrons of Fe_{II} (upper lines) and Fe_{I} (lower lines, magnified by a factor 2) in $\text{LaFe}_{11.5}\text{Si}_{1.5}$. FM state: blue line; PM state: red line; FSM state: dashed turquoise line. The quasigap at the Fermi energy E_{Fermi} for the FM state is indicated by the vertical black arrow. For clarity, all $D(E)$ were broadened by convoluting the data with a Gaussian distribution function of width $\sigma = 0.1$ eV.

in Fig. 4(d). In the experiment, the jump at T_C amounts to $\Delta C_{\text{vib}} = +0.024k_B/\text{Fe atom}$ [or $+2.7 \text{ J}/(\text{kg K})$] for the FM-to-PM transition [Fig. 4(b)]. This value should be compared with the change in specific heat, ΔC_{vib} (theory) between the computed FSM and FM states, which can be estimated from Fig. 4(d) to be ΔC_{vib} (theory) = $+0.052k_B/\text{Fe atom}$ [or $+6.2 \text{ J}/(\text{kg K})$] at T_C . The computed increase in specific heat ΔC_{vib} (theory) is found to be by a factor of ~ 2.2 larger than the experimental jump ΔC_{lat} . Nevertheless, we find qualitative agreement between theory and experiment with respect to the change in vibrational specific heat at the FM-to-PM transition.

The rather abrupt changes observed in the phonon spectrum when the temperature crosses the magnetostructural transition temperature T_C are closely related to a distinct modification of the electronic density of states $D(E_F)$ at the Fermi energy E_F [46,76]. These are illustrated in Fig. 5, where we show the partial electronic density of states $D(E)$ for the minority d channel of Fe_{I} and Fe_{II} of $\text{LaFe}_{11.5}\text{Si}_{1.5}$, computed by DFT for the FM, PM, and the FSM state, respectively. For both Fe sites, $D(E)$ for the FM state (blue line) exhibits a nearly half filled minority channel and, more importantly, a deep mid- d -band minimum found right at the Fermi level E_F (see vertical arrow in Fig. 5). This low $D(E)$ at E_F stabilizes the FM state and reduces electronic screening of perturbations from displaced Fe atoms. Unlike $D(E_F)$ for the FM state, the Fe-resolved minority band $D(E)$ for the PM phase (thin red lines) does not exhibit the d -band minimum right at E_F , but approximately 0.6 eV below. As discussed earlier in the context of A15 compounds, alloys with order-disorder transitions, and narrow band-gap semiconductors [96–99], the higher availability of electronic states at E_F results in enhanced electronic screening of perturbations from a displaced atom, termed *adiabatic electron-phonon coupling*, which can cause a substantial softening of the vibrational modes. Here, this mechanism apparently results in the phonon softening in the PM state and, moreover, to the disappearance of the phonon mode at ~ 27 meV, as observed by both theory and experiment. It is important to note that also for the FSM calculations, the minimum in the minority d -band $D(E)$

(turquoise dashed line in Fig. 5) is shifted below E_F , albeit not as pronounced as for the PM case, as a consequence of the decreased exchange splitting. Accordingly, we see again a redshift of the Fe-VDOS and also the ~ 27 -meV phonon peak is absent in the FSM computation (Fig. 2, red line). This proves that spin waves or magnetic disorder are not directly related to the strong modification of the Fe-VDOS at T_C . The softening can be readily explained by the decrease of the Fe moments, which change in magnitude at T_C . This moves the stabilizing minimum in the minority DOS away from E_F , leading to the appearance of strong adiabatic electron-phonon coupling. Thus, the disruptive changes in the VDOS around T_C are another expression of the itinerant electron metamagnetism, which is characteristic for this magnetocaloric system. Therefore, any theoretical description of the magnetostructural transition in $\text{La}(\text{Fe},\text{Si})_{13}$ -based compounds definitely requires the consideration of electronic band-structure modifications across that transition.

Our observations in the preceding paragraph indicate that the discrepancy between our work and previous phenomenological descriptions [42,43,50] regarding the counteracting role of ΔS_{vib} might be traced back to the modeling of the coupling between magnetism and lattice degrees of freedom. In the spirit of the Bean-Rodbell model it is often assumed that the molecular field, which derives from the magnetic exchange interactions, depends mainly on the interatomic spacing, as for instance predicted by the Bethe-Slater curve [43]. In turn, lattice degrees of freedom depend on the atomic volume as well, which is often modeled in terms of a conventional Grüneisen behavior. Our work shows, however, that in $\text{La}(\text{Fe},\text{Si})_{13}$ -based compounds a different mechanism based on adiabatic electron-phonon coupling dominates the magnetoelastic interactions, which derives solely from local changes in the electronic structure [46], which are by definition not considered in a Bean-Rodbell-type model. A pragmatic workaround for a first-order transition could be—similar as for a magnetostructural transition with a substantial change in lattice symmetry and elastic properties—to use a Debye model with different Debye temperatures Θ_D for both phases to describe their vibrational properties. Appropriate values for Θ_D are provided by us in the next section. For accurate results, the appropriate cross-coupling terms to the entropy change, which involve all relevant combinations of the different degrees of freedom, must be formulated, which is still an important open task.

C. Other thermodynamic quantities via NRIXS

Using the experimental Fe-partial VDOS, $g(E)$, we have derived several other important vibrational thermodynamic properties of the Fe subsystem. These quantities are calculated by integration of $g(E)$ with various energy weights, as given by Eqs. (3)–(11) in the Supplemental Material. The calculated quantities and their temperature dependence are the mean-square atomic displacement $\langle z^2 \rangle$ [Figs. 6(a) and 6(b)], the mean-square atomic velocity $\langle v_z^2 \rangle$ [Figs. 6(c) and 6(d)], the mean atomic force constant K [Fig. 6(e)], and the Debye temperature θ_D [Fig. 6(f)]. The Debye temperature was calculated from the Lamb-Mössbauer factor f_{LM} (see Fig. S6 in the SM). All quantities shown in Fig. 6 are directional quantities, i.e., they are given along the incident photon direction (z direction)

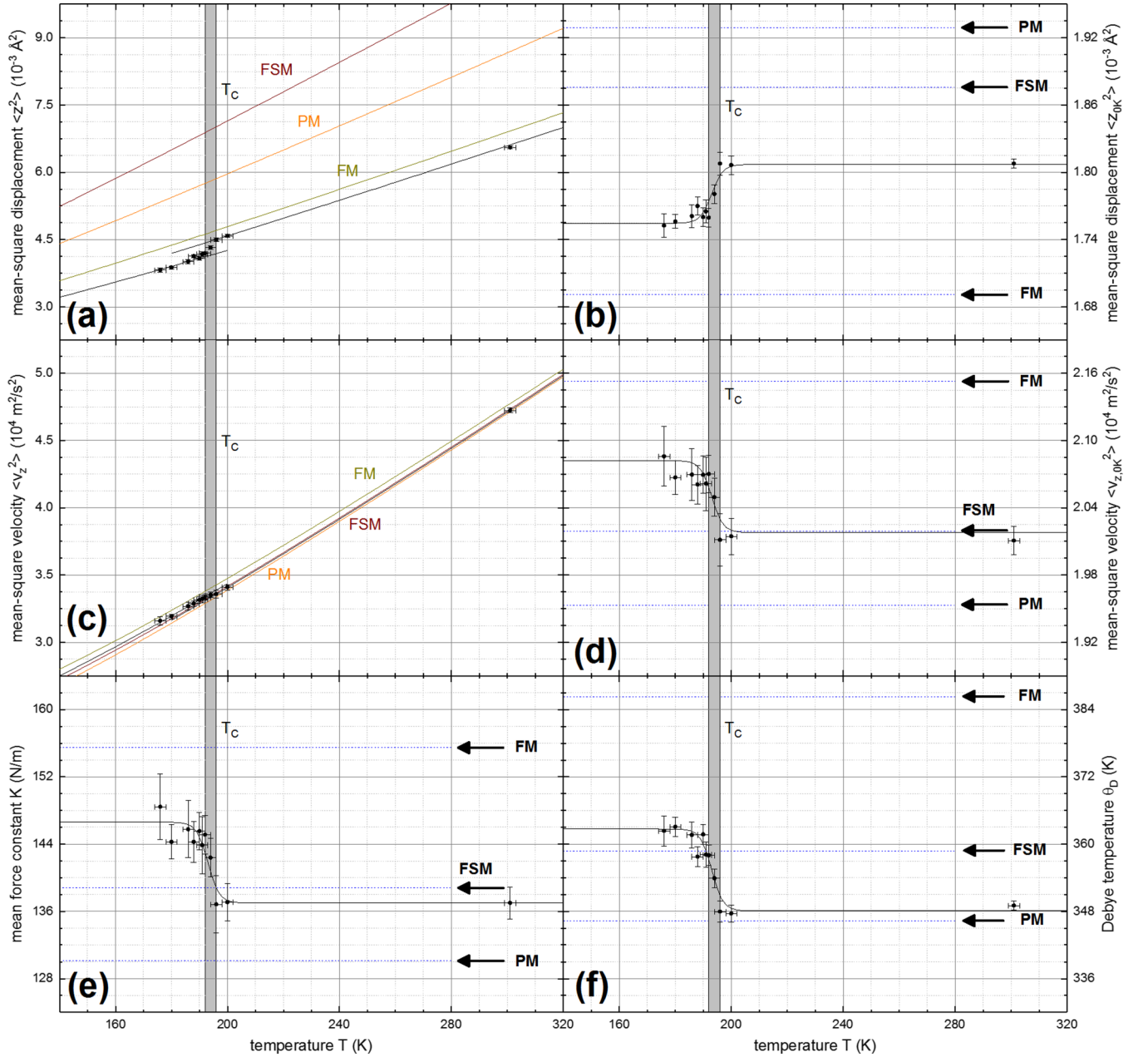


FIG. 6. Temperature dependence of various Fe-partial thermodynamic vibrational quantities obtained from NRIXS. T is the measurement temperature. The experimental data (black dots) were obtained from the experimental VDOS, $g(E)$, measured at temperature T , and by energy-weighted integration of $g(E)$ according to Eqs. (3), (5), and (7), respectively, in the Supplemental Material (SM). (a),(b) Mean-square atomic displacement, $\langle z^2 \rangle$, derived from the Lamb-Mössbauer factor, f_{LM} (see Fig. S6 in the SM); (c),(d) Mean-square atomic velocity $\langle v_z^2 \rangle$, derived from the mean kinetic energy E_{kin} (see Fig. S6 in the SM); the quantities in (b) and (d) are the zero-point quantities derived by extrapolating to $T = 0$ K using $g(E)$ at the measurement T and energy-weighted integration of $g(E)$ according to Eqs. (3) and (5), respectively, in the SM. (e) Mean atomic force constant K ; (f) Debye temperature θ_D derived from the Lamb-Mössbauer factor f_{LM} (see Fig. S6 in the SM). The black lines drawn in (a) are calculated from the thermodynamic relation for $\langle z^2 \rangle(T)$, Eq. (3) (see SM), using the experimental $g(E)$ for the FM and PM region, respectively. The line drawn in (c) follows Eq. (5) for $\langle v_z^2 \rangle(T)$ (see SM). All other black lines serve as a guide to the eye. For comparison with the experimental results, we show also the DFT-based computed T dependence of $\langle z^2 \rangle$ in (a), and $\langle v_z^2 \rangle$ in (c) for the FM state (olive line), the FSM state (magenta line), and the PM state (orange line) using the thermodynamic relations Eqs. (3)–(6), respectively (see SM). The computed zero-point quantities ($T \rightarrow 0$ K) $\langle z_{0K}^2 \rangle$ in (b), $\langle v_{z,0K}^2 \rangle$ in (d), K in (e), and θ_D in (f) were obtained at $T = 1$ K as an approximation and are indicated by black arrows for the FM, FSM, and PM state, respectively. The anomaly near T_C of $\langle v_z^2 \rangle$ in Fig. 6(c) [and also of E_{kin} in Fig. S6(c) in the SM] appears to be small. This observation can be understood by the fact that according to kinetic gas theory both $\langle v_z^2 \rangle$ and E_{kin} are dominated by the proportionality to temperature T , and apparently the magnetoelastic coupling induces only a small disturbance in this T dependence near T_C .

and, thus, they are given for one vibrational degree of freedom [68]. This is in contrast to the quantities $S(T)$ and $C_V(T)$ shown in Fig. 4, which are given for three vibrational degrees of freedom.

Some quantities, as shown in Fig. 6(b) ($\langle z^2 \rangle$) and Fig. 6(d) ($\langle v_z^2 \rangle$), were obtained by extrapolation from the measurement temperature T to $T = 0$ K, using Eqs. (3) and (5), respectively, as given in the SM. Thus, Figs. 6(b) and 6(d) exhibit the extrapolated zero-point vibrational quantities. Such an extrapolation certainly is an approximation only, since the relations used [Eqs. (3)–(5) in the SM] are strictly valid for constant volume only, and since it is assumed that $g(E)$ is independent of T in the FM and PM region, respectively. However, in view of the fact that thermal lattice expansion is negligible below T_C (Invar-type behavior) [22–24,27,88] and is relatively small in the PM region [22–24], such an approximation appears to be justified.

Furthermore, several thermodynamic properties may be derived also from the raw experimental data (NRIXS spectra), i.e., from the probability of inelastic absorption $S(E)$, which is obtained from the measured NRIXS spectrum after subtraction of the elastic (central) peak and proper normalization [100]. The Lamb-Mössbauer factor is given by the zeroth energy moment of the distribution $S(E)$, E_{kin} by the second moment, and K by the third moment [68,100]. For the analysis we have used Eqs. (8)–(11) in the SM section. Our results obtained from the analysis of the energy moments (not shown) agree very well with the corresponding data in Fig. 6 obtained from the energy-weighted integration of $g(E)$.

It is evident from Fig. 6 that all calculated quantities exhibit anomalies near the magnetostructural transition due to the modification of $g(E)$ that occurs across T_C . (Other Fe-partial thermodynamic properties are displayed in Fig. S6 of the SM section.) In particular, upon the FM-to-PM transition, the mean-square atomic displacement ($\langle z^2 \rangle$) and its zero-point value ($\langle z_{0K}^2 \rangle$) increase at T_C , whereas the zero-point mean-square velocity ($\langle v_{z,0K}^2 \rangle$), the mean atomic force constant (K), and the Debye temperature (θ_D) all decrease. Related quantities, i.e., the Lamb-Mössbauer factor (f_{LM}) and its zero-point value as well as the zero-point mean kinetic energy (E_{kin}) of the Fe atom all show a decrease in magnitude within a small temperature interval upon heating from the FM to the PM state, as is demonstrated in Fig. S6 of the SM. Our findings in Fig. 6 are a clear manifestation of strong lattice softening that occurs upon heating magnetocaloric $\text{LaFe}_{11.6}\text{Si}_{1.4}$ across T_C . The value of the Debye temperature [derived from fitting the Lamb-Mössbauer factor, $f_{LM}(T)$, Fig. S6 in the SM] is found to drop by $\sim 4\%$ from $\theta_D = (363 \pm 2)$ K in the FM phase to $\theta_D = (348 \pm 2)$ K in the PM phase. A similar reduction of θ_D was obtained previously for our $\text{LaFe}_{11.6}\text{Si}_{1.4}$ sample for the entropy-related Debye temperature, i.e., from $\theta_D = 371$ K in the FM region to 360 K in the PM region [46]. There is fair agreement between our θ_D result in the FM state and some corresponding literature values: $\theta_D = 361$ and 347 K for $\text{LaFe}_{11.8}\text{Si}_{1.2}$ and $\text{LaFe}_{11.4}\text{Si}_{1.6}$ in the FM phase, respectively, from low-temperature specific-heat measurements [38], and $\theta_D = 317, 330,$ and 336 K for $\text{LaFe}_{11.7}\text{Si}_{1.3}$, $\text{LaFe}_{11.3}\text{Si}_{1.7}$, and $\text{LaFe}_{11.0}\text{Si}_{2.0}$ in the FM phase, respectively, from T -dependent Mössbauer spectroscopical studies [101]. However, for the FM state, our θ_D value is at odds with the corresponding Debye

temperatures in the range of 220–230 K given in Refs. [41,50]. To the best of our knowledge, no Debye temperature of $\text{La}(\text{Fe},\text{Si})_{13}$ in the PM phase has been reported in the literature.

The excellent agreement between the experimental and calculated VDOS, as shown in Fig. 2, motivates us to quantitatively compare the derived thermodynamic quantities as well. In Fig. 6 and Fig. S6 (see the SM), we display also the relevant DFT-based computed thermodynamic quantities as a function of temperature, for comparison with the experimental (NRIXS) results. All in all, we see the qualitative changes in all quantities well reproduced, sometimes even on a nearly quantitative level. The T dependence of all computed quantities nicely confirms the same jumplike tendencies as observed for the experimental thermodynamic quantities. Generally, the agreement between theory and experiment is very good for the FM state ($T \leq T_C$). However, for the FSM and PM state (which approximately represent the paramagnetic state at $T > T_C$) the deviation from the experimental data is found to be larger, with the FSM description remaining somewhat closer to experiment. We ascribe most of the discrepancies to our $T = 0$ description of the different magnetic phases in the framework of density functional theory, which neglects, for instance, dynamic spin fluctuations and phonon-phonon interactions. In some quantities, however, like the mean-square displacement in Fig. 6(a), larger discrepancies are encountered. This is related to the fact that the expressions for these quantities involve low (negative) moments of $g(E)$. These emphasize the low-energy region ($E \leq 5$ meV) of the VDOS, where we expect both the theoretical and NRIXS description of lattice vibrations to be systematically less accurate compared to the higher energy range in the experiment due to the subtraction of the elastic (central) peak in the NRIXS spectra. This indicates that for the quantitative analysis of thermodynamic data derived from $g(E)$, particular care must be taken that the vibrational excitations are sufficiently well described in the relevant energy range. In turn, the comparison of experimental data with theoretical modeling provides a reasonable estimate with respect to the reliability of a conclusion derived from a particular quantity.

IV. SUMMARY AND CONCLUSIONS

For the giant magnetocaloric compound $\text{LaFe}_{11.6}\text{Si}_{1.4}$, we precisely measured the Fe-partial vibrational (phonon) density of states (VDOS) by ^{57}Fe NRIXS in a magnetic field of $\mu_0 H \sim 0.7$ T. From the VDOS and using textbook equations from thermodynamics, we calculated the vibrational entropy $S_{\text{vib}}(T)$ and the vibrational specific heat $C_{\text{vib}}(T)$ of the Fe subsystem in a small temperature range across the Curie temperature T_C at the isostructural first-order magnetostructural phase transition. Our results reveal prominent changes in the VDOS near a phonon energy of ~ 27 meV and a remarkable overall redshift by -1.5% of the phonon spectrum within a narrow temperature interval of ~ 12 K across T_C . Both observations are a manifestation of substantial magnetoelastic coupling at the atomic scale in the $\text{LaFe}_{11.6}\text{Si}_{1.4}$ compound, as also illustrated in our previous work [46]. $S_{\text{vib}}(T)$ as well as $C_{\text{vib}}(T)$ exhibit a jump by $\Delta S_{\text{vib}} = +0.060k_B/\text{Fe atom}$ [or $+6.9$ J/(kg K)] and by $\Delta C_{\text{vib}} = +0.024k_B/\text{Fe atom}$ [or $+2.7$ J/(kg K)] upon heating across $T_C \sim 192$ K. Our experimental findings are compared

with theoretical results using DFT-based calculations for the FM and PM states, and, in addition, for the theoretical FSM state. Excellent agreement is observed between the experimental and computed Fe VDOS in the FM state, and between the experimental VDOS of the PM state and the computed FSM VDOS. The experimental and computed changes ΔS_{vib} and ΔC_{vib} , respectively, are found to be in sensible agreement. The origin of the magnetoelastic coupling is attributed to distinct modifications in the electronic minority d band across the phase transition, and in particular to a change of the minority electronic density of states $D(E_F)$ at the Fermi energy E_F , which leads to adiabatic electron-phonon coupling. Our theoretical finding emphasizes the itinerant character of the 3d electrons in $\text{La}(\text{Fe},\text{Si})_{13}$ and is in line with the concept by Fujita *et al.* [23] of an itinerant-electron metamagnetic transition. Our computed redistribution of electron-spin density across the phase transition is reminiscent of the origin of the Invar effect in $\text{Fe}_{65}\text{Ni}_{35}$ (and other ferrous alloys), where redistribution of the Fe spin density from a high-spin to a low-spin Fe moment state has been inferred in order to explain the Invar-type thermal-expansion anomaly [80,93,102,103]. In fact, in the FM phase of $\text{La}(\text{Fe},\text{Si})_{13}$ the thermal-expansion coefficient is largely reduced or even negative [24,27,84,88,104], which presents similarities with the Invar effect. The abrupt increase ΔS_{vib} of the Fe subsystem at the FM-to-PM transition, observed both experimentally and theoretically, is substantial and contributes significantly to the increase in the total isothermal entropy change, ΔS_{iso} , at T_C . Our work indicates that ΔS_{vib} of the Fe subsystem is a significant factor responsible for the outstand-

ing magnetocaloric properties of $\text{La}(\text{Fe},\text{Si})_{13}$ compounds. Other thermodynamic vibrational quantities, inferred from our NRIXS results, were found to exhibit striking anomalies near the magnetostructural transition at T_C . These findings are a manifestation of strong lattice softening occurring upon heating magnetocaloric $\text{LaFe}_{11.6}\text{Si}_{1.4}$ across T_C . Comparison of the maximum literature value of $\Delta S_{\text{iso}} = +24 \text{ J}/(\text{kg K})$ [12] with our data demonstrates that ΔS_{vib} obtained by NRIXS is a sizable quantity and contributes directly and cooperatively with at least 29% to the total isothermal entropy change ΔS_{iso} at the phase transition of $\text{LaFe}_{11.6}\text{Si}_{1.4}$.

ACKNOWLEDGMENTS

We are grateful to U. von Hörsten for outstanding technical assistance and A. Terwey (Duisburg-Essen) for assistance in the application of the PHOENIX program. This work has been supported by the Deutsche Forschungsgemeinschaft in the framework of the priority program SPP 1599 (Grants No. GR3498/3-2, No. GU514/6-2, and No. WE2623/12-2), SPP 1681 (Grant No. WE2623/7-1), FOR 1509 (Grant No. WE2623/13-2), SFB 1242 (project A5), and by Stiftung Mercator (MERCUR). This research used resources of the Advanced Photon Source, a US Department of Energy (DOE) Office of Science User Facility operated for the DOE Office of Science by Argonne National Laboratory under Contract No. DE-AC02-06CH11357. The calculations were carried out on the Cray XT6/m and Opterox supercomputer systems of the University of Duisburg-Essen.

-
- [1] S. Fähler and V. K. Pecharsky, *MRS Bull.* **43**, 264 (2018).
- [2] A. M. Tishin and Y. I. Spichkin, *The Magnetocaloric Effect and its Applications*, Series in Condensed Matter Physics (Institute of Physics, Bristol, 2003).
- [3] K. A. Gschneidner, Jr., V. K. Pecharsky, and A. O. Tsokol, *Rep. Prog. Phys.* **68**, 1479 (2005).
- [4] C. Zimm, A. Broeder, J. Chell, A. Sternberg, A. Fujita, S. Fujieda, and K. Fukamichi, *Int. J. Refrig.* **29**, 1302 (2006).
- [5] S. L. Russek and C. Zimm, *Int. J. Refrig.* **29**, 1366 (2006).
- [6] O. Gutfleisch, M. A. Willard, E. Brück, C. H. Chen, S. G. Sankar, and J. P. Liu, *Adv. Mater.* **23**, 821 (2011).
- [7] N. H. Dung, Z. Q. Ou, L. Caron, L. Zhang, D. T. Cam Thanh, G. A. de Wijs, R. A. de Groot, K. H. Buschow, and E. Brück, *Adv. Energy Mater.* **1**, 1215 (2011).
- [8] S. Fähler, U. K. Röbber, O. Kastner, J. Eckert, G. Eggeler, H. Emmerich, P. Entel, S. Müller, E. Quandt, and K. Albe, *Adv. Eng. Mater.* **14**, 10 (2012).
- [9] K. G. Sandeman, *Scr. Mater.* **67**, 566 (2012).
- [10] J. Liu, T. Gottschall, K. P. Skokov, J. D. Moore, and O. Gutfleisch, *Nat. Mater.* **11**, 620 (2012).
- [11] M. F. J. Boeije, P. Roy, F. Guillou, H. Yibole, X. F. Miao, L. Caron, D. Banerjee, N. H. van Dijk, R. A. de Groot, and E. Brück, *Chem. Mater.* **28**, 4901 (2016).
- [12] S. Fujieda, A. Fujita, and K. Fukamichi, *Appl. Phys. Lett.* **81**, 1276 (2002).
- [13] G. H. Wen, R. K. Zheng, X. X. Zhang, W. H. Wang, J. L. Chen, and G. H. Wu, *J. Appl. Phys.* **91**, 8537 (2002).
- [14] F.-X. Hu, M. Ilyn, A. M. Tishin, J. R. Sun, G. J. Wang, Y. F. Chen, F. Wang, Z. H. Cheng, and B. G. Shen, *J. Appl. Phys.* **93**, 5503 (2003).
- [15] S. Fujieda, Y. Hasegawa, A. Fujita, and K. Fukamichi, *J. Magn. Magn. Mater.* **272-276**, 2365 (2004).
- [16] J. Liu, M. Krautz, K. Skokov, T. G. Woodstock, and O. Gutfleisch, *Acta Mater.* **59**, 3602 (2011).
- [17] O. Gutfleisch, T. Gottschall, M. Fries, D. Benke, I. Radulov, K. P. Skokov, H. Wende, M. Gruner, M. Acet, P. Entel, and M. Farle, *Phil. Trans. R. Soc. London A* **374**, 20150308 (2016).
- [18] F. Wang, G.-J. Wang, F.-X. Hu, A. Kurbakov, B.-G. Shen, and Z.-H. Cheng, *J. Phys.: Condens. Matter* **15**, 5269 (2003).
- [19] X. B. Liu, Z. Altounian, and D. H. Ryan, *J. Phys.: Condens. Matter* **15**, 7385 (2003).
- [20] H. H. Hamdeh, H. Al-Ghanem, W. M. Hikal, S. M. Taher, J. C. Ho, D. T. K. Anh, N. P. Thuy, N. H. Duc, and P. D. Thang, *J. Magn. Magn. Mater.* **269**, 404 (2004).
- [21] M. Rosca, M. Balli, D. Fruchard, D. Gignoux, E. K. Hlil, S. Miraglia, B. Ouladdiaf, and P. Wolfers, *J. Alloys Compd.* **490**, 50 (2010).
- [22] K. Fukamichi and A. Fujita, *J. Mater. Sci. Technol.* **16**, 167 (2000).
- [23] A. Fujita, S. Fujieda, K. Fukamichi, H. Mitamura, and T. Goto, *Phys. Rev. B* **65**, 014410 (2001).
- [24] H. Chang, J.-K. Liang, B.-G. Shen, L.-T. Yang, F. Wang, N.-X. Chen, and G.-H. Rao, *J. Phys. D: Appl. Phys.* **36**, 160 (2003).

- [25] Ll. Mañosa, D. González-Alonso, A. Planes, M. Barrio, J.-L. Tamarit, I. S. Titov, M. Acet, A. Bhattacharyya, and S. Majumdar, *Nat. Commun.* **2**, 595 (2011).
- [26] S. Fujieda, A. Fujita, K. Fukamichi, Y. Yamazaki, and Y. Iijima, *Appl. Phys. Lett.* **79**, 653 (2001).
- [27] A. Fujita, S. Fujieda, Y. Hasegawa, and K. Fukamichi, *Phys. Rev. B* **67**, 104416 (2003).
- [28] Y.-F. Chen, F. Wang, B.-G. Shen, F.-X. Hu, J.-R. Sun, G.-J. Wang, and Z.-H. Cheng, *J. Phys.: Condens. Matter* **15**, L161 (2003).
- [29] J. Lyubina, K. Nenkov, L. Schultz, and O. Gutfleisch, *Phys. Rev. Lett.* **101**, 177203 (2008).
- [30] L. Jia, J. R. Sun, J. Shen, B. Gao, T. Y. Zhao, H. W. Zhang, F. X. Hu, and B. G. Shen, *J. Alloys Compd.* **509**, 5804 (2011).
- [31] C. S. Teixeira, M. Krautz, J. D. Moore, K. Skokov, J. Liu, P. A. P. Wendhausen, and O. Gutfleisch, *J. Appl. Phys.* **111**, 07A927 (2012).
- [32] M. Krautz, J. D. Moore, K. P. Skokov, J. Liu, C. S. Teixeira, R. Schäfer, L. Schultz, and O. Gutfleisch, *J. Appl. Phys.* **112**, 083918 (2012).
- [33] O. L. Baumfeld, Z. Gercsi, M. Krautz, O. Gutfleisch, and K. G. Sandeman, *J. Appl. Phys.* **115**, 203905 (2014).
- [34] F. Wang, Y. F. Chen, G. J. Wang, J. R. Sun, and B. G. Shen, *Chin. Phys.* **12**, 911 (2003).
- [35] A. Barcza, M. Katter, V. Zellmann, S. Russek, S. Jacobs, and C. Zimm, *IEEE Trans. Magn.* **47**, 3391 (2011).
- [36] J. Liu, J. D. Moore, K. P. Skokov, M. Krautz, K. Löwe, A. Barcza, M. Katter, and O. Gutfleisch, *Scr. Mater.* **67**, 584 (2012).
- [37] M. Krautz, K. Skokov, T. Gottschall, C. S. Teixeira, A. Waske, J. Liu, L. Schultz, and O. Gutfleisch, *J. Alloys Compd.* **598**, 27 (2014).
- [38] E. Lovell, L. Ghivelder, A. Nicotina, J. Turcaud, M. Bratko, A. D. Caplin, V. Basso, A. Barcza, M. Katter, and L. F. Cohen, *Phys. Rev. B* **94**, 134405 (2016).
- [39] T. Zhang, C.-Y. Wang, L. Li, Y. Zhang, and C.-L. Liu, *J. Iron Steel Res. Int.* **24**, 462 (2017).
- [40] We would like to mention that the *static* configurational entropy S_{conf} which depends on the long-range and/or short-range chemical order parameters according to its statistical definition [see, e.g., C. Kittel, *Introduction to Solid State Physics*, 5th ed. (John Wiley & Sons, New York, London, Sydney, Toronto, 1976), p. 561], does not change across the FM-to-PM magnetostructural phase transition of the $\text{LaFe}_{13-x}\text{Si}_x$ compound, because this transition is of isostructural nature, where the chemical order parameters and the symmetry of the crystallographic unit cell remain unchanged, whereas only an isostructural contraction of the unit cell occurs. The low transition temperature T_C of only approximately 192 K prevents atomic diffusion or atomic site exchange and, consequently, the chemical order parameters do not change across this phase transition, leaving the static configurational entropy constant across T_C . Thus, the static configurational entropy S_{conf} does not contribute to the magnetocaloric effect.
- [41] P. J. von Ranke, N. A. de Oliveira, C. Mello, A. M. Carvalho, and S. Gama, *Phys. Rev. B* **71**, 054410 (2005).
- [42] M. Piazza, C. Benati, C. Curcio, M. Kuepferling, and V. Basso, *J. Magn. Magn. Mater.* **400**, 349 (2016).
- [43] V. Basso, M. Piazza, C. Bennati, and C. Curcio, *Phys. Status Solidi B* **255**, 1700278 (2018).
- [44] C. P. Bean and D. S. Rodbell, *Phys. Rev.* **126**, 104 (1962).
- [45] T. Mukherjee, S. Michalski, R. Skomski, D. J. Sellmyer, and C. Binek, *Phys. Rev. B* **83**, 214413 (2011).
- [46] M. E. Gruner, W. Keune, B. Roldan Cuenya, C. Weis, J. Landers, S. I. Makarov, D. Klar, M. Y. Hu, E. E. Alp, J. Zhao, M. Krautz, O. Gutfleisch, and H. Wende, *Phys. Rev. Lett.* **114**, 057202 (2015).
- [47] K. Morrison, J. Lyubina, J. D. Moore, A. D. Caplin, K. G. Sandeman, O. Gutfleisch, and L. F. Cohen, *J. Phys. D: Appl. Phys.* **43**, 132001 (2010).
- [48] D. W. Cooke, F. Hellman, C. Baldasseroni, C. Bordel, S. Moyerman, and E. E. Fullerton, *Phys. Rev. Lett.* **109**, 255901 (2012).
- [49] M. Wolloch, M. E. Gruner, W. Keune, P. Mohn, J. Redinger, F. Hofer, D. Suess, R. Podloucky, J. Landers, S. Salamon, F. Scheibel, D. Spoddig, R. Witte, B. Roldan Cuenya, O. Gutfleisch, M. Y. Hu, J. Zhao, T. Toellner, E. E. Alp, M. Siewert *et al.*, *Phys. Rev. B* **94**, 174435 (2016).
- [50] L. Jia, G. J. Liu, J. R. Sun, H. W. Zhang, F. X. Hu, C. Dong, G. H. Rao, and B. G. Shen, *J. Appl. Phys.* **100**, 123904 (2006).
- [51] V. K. Pecharsky, G. A. Gschneidner, Jr., Y. Mudryk, and D. Paudyal, *J. Magn. Magn. Mater.* **321**, 3541 (2009).
- [52] K. S. Singwi and A. Sjölander, *Phys. Rev.* **120**, 1093 (1960).
- [53] R. Röhlberger, *Nuclear Condensed Matter Physics with Synchrotron Radiation, Basic Principles, Methodology and Applications*, Springer Tracts in Modern Physics Vol. 208 (Springer, Berlin, Heidelberg, 2004), Chap. 5.
- [54] See Supplemental Material at <http://link.aps.org/supplemental/10.1103/PhysRevB.98.024417>, which includes Refs. [2,3,9,52,66–71,84,100,105–117].
- [55] A. R. Williams, V. L. Moruzzi, J. Kübler, and K. Schwarz, *Bull. Am. Phys. Soc.* **29**, 278 (1984).
- [56] K. Schwarz and P. Mohn, *J. Phys. F: Met. Phys.* **14**, L129 (1984).
- [57] P. H. Dederichs, S. Blügel, R. Zeller, and H. Akai, *Phys. Rev. Lett.* **53**, 2512 (1984).
- [58] V. L. Moruzzi, P. M. Marcus, K. Schwarz, and P. Mohn, *Phys. Rev. B* **34**, 1784 (1986).
- [59] V. K. Pecharsky and K. A. Gschneidner, Jr., *J. Magn. Magn. Mater.* **200**, 44 (1999).
- [60] V. K. Pecharsky and K. A. Gschneidner, Jr., *J. Appl. Phys.* **86**, 565 (1999).
- [61] V. K. Pecharsky, A. P. Holm, K. A. Gschneidner, Jr., and R. Rink, *Phys. Rev. Lett.* **91**, 197204 (2003).
- [62] M. Seto, Y. Yoda, S. Kikuta, X. W. Zhang, and M. Ando, *Phys. Rev. Lett.* **74**, 3828 (1995).
- [63] W. Sturhahn, T. S. Toellner, E. E. Alp, X. W. Zhang, M. Ando, Y. Yoda, S. Kikuta, M. Seto, C. W. Kimball, and B. Dabrowski, *Phys. Rev. Lett.* **74**, 3832 (1995).
- [64] A. I. Chumakov, R. Rüffer, H. Grünsteudel, H. F. Grünsteudel, G. Grübel, J. Metge, O. Leupold, and H. A. Goodwin, *Europhys. Lett.* **30**, 427 (1995).
- [65] T. S. Toellner, *Hyperfine Interact.* **125**, 3 (2000).
- [66] W. Sturhahn, *Hyperfine Interact.* **125**, 149 (2000).
- [67] W. Sturhahn, *J. Phys.: Condens. Matter* **16**, S497 (2004).
- [68] M. Y. Hu, T. S. Toellner, N. Dauphas, E. E. Alp, and J. Zhao, *Phys. Rev. B* **87**, 064301 (2013).
- [69] G. Grimval, *Thermophysical Properties of Materials*, Selected Topics in Solid State Physics Vol. 18 (North-Holland, Amsterdam, 1986).

- [70] B. Fultz, *Prog. Mater. Sci.* **55**, 247 (2010).
- [71] S. Stankov, M. Miglierini, A. I. Chumakov, I. Sergueev, Y. Z. Yue, B. Sepiol, P. Vec, L. Hu, and R. Rüffer, *Phys. Rev. B* **82**, 144301 (2010).
- [72] G. Kresse and J. Furthmüller, *Phys. Rev. B* **54**, 11169 (1996).
- [73] G. Kresse and D. Joubert, *Phys. Rev. B* **59**, 1758 (1999).
- [74] J. P. Perdew, *Electronic Structure of Solids '91*, edited by P. Ziesche and H. Eschrig (Akademie Verlag, Berlin, 1991).
- [75] D. Alfé, *Comput. Phys. Commun.* **180**, 2622 (2009).
- [76] M. E. Gruner, W. Keune, J. Landers, S. Salamon, M. Krautz, J. Zhao, M. Y. Hu, T. Toellner, E. E. Alp, O. Gutfleisch, and H. Wende, *Phys. Status Solidi B* **255**, 1700465 (2018).
- [77] P. M. Marcus and V. L. Moruzzi, *Phys. Rev. B* **38**, 6949 (1988).
- [78] M. Podgorny, *Physica B* **161**, 105 (1990).
- [79] J. Häglund, *Phys. Rev. B* **47**, 566 (1993).
- [80] P. Entel, E. Hoffmann, P. Mohn, K. Schwarz, and V. L. Moruzzi, *Phys. Rev. B* **47**, 8706 (1993).
- [81] M. D. Kuz'min and M. Richter, *Phys. Rev. B* **76**, 092401 (2007).
- [82] A. Fujita and H. Yako, *Scr. Mater.* **67**, 578 (2012).
- [83] Z. Gercsi, N. Fuller, K. G. Sandeman, and A. Fujita, *J. Phys. D: Appl. Phys.* **51**, 034003 (2018).
- [84] F.-X. Hu, B.-G. Shen, J.-R. Sun, and Z.-H. Cheng, *Appl. Phys. Lett.* **78**, 3675 (2001).
- [85] C. Kittel, *Introduction to Solid State Physics*, 2nd ed. (John Wiley & Sons, New York, London, 1956), p. 154 .
- [86] C. V. Pandya, P. R. Vyas, T. C. Pandya, and V. B. Gohel, *Bull. Mater. Sci.* **25**, 63 (2002).
- [87] N. W. Ashcroft and N. D. Mermin, in *Solid State Physics* (W. B. Saunders, Philadelphia, 1976), p. 493 .
- [88] A. Fujita, K. Fukamichi, J.-T. Wang, and Y. Kawazoe, *Phys. Rev. B* **68**, 104431 (2003).
- [89] E. Fawcett, *J. Phys.: Condens. Matter* **1**, 203 (1989).
- [90] Ll. Mañosa, G. A. Saunders, H. Rahdi, U. Kawald, J. Pelzl, and H. Bach, *Phys. Rev. B* **45**, 2224 (1992).
- [91] R. Mittal, S. L. Chaplot, H. Schober, and T. A. Mary, *Phys. Rev. Lett.* **86**, 4692 (2001).
- [92] R. Mittal, M. K. Gupta, and S. L. Chaplot, *Prog. Mater. Sci.* **92**, 360 (2018).
- [93] E. F. Wassermann, in *Ferromagnetic Materials*, edited by K. H. J. Buschow and E. P. Wohlfarth (Elsevier, Amsterdam, 1990), Vol. 5, Chap. 3, p. 237, and references therein.
- [94] S. I. Makarov, M. Krautz, S. Salamon, K. Skokov, C. S. Teixeira, O. Gutfleisch, H. Wende, and W. Keune, *J. Phys. D: Appl. Phys.* **48**, 305006 (2015).
- [95] M. Seto, S. Kitao, Y. Kobayashi, R. Haruki, Y. Yoda, T. Mitsui, and T. Ishikawa, *Phys. Rev. Lett.* **91**, 185505 (2003).
- [96] O. Delaire, M. S. Lucas, J. A. Muñoz, M. Kresch, and B. Fultz, *Phys. Rev. Lett.* **101**, 105504 (2008).
- [97] M. S. Lucas, J. A. Muñoz, O. Delaire, N. D. Markovskiy, M. B. Stone, D. L. Abernathy, I. Halevy, L. Mauger, J. B. Keith, M. L. Winterrose, Y. Xiao, M. Lerche, and B. Fultz, *Phys. Rev. B* **82**, 144306 (2010).
- [98] O. Delaire, K. Marty, M. B. Stone, P. R. C. Kent, M. S. Lucas, D. L. Abernathy, D. Mandrus, and B. C. Sales, *Proc. Natl. Acad. Sci. USA* **108**, 4725 (2011).
- [99] J. A. Muñoz, M. S. Lucas, O. Delaire, M. L. Winterrose, L. Mauger, C. W. Li, A. O. Sheets, M. B. Stone, D. L. Abernathy, Y. Xiao, P. Chow, and B. Fultz, *Phys. Rev. Lett.* **107**, 115501 (2011).
- [100] R. Rüffer and A. I. Chumakov, *Hyperfine Interact.* **128**, 255 (2000).
- [101] G.-J. Wang, F. Wang, N.-L. Di, B.-G. Shen, and Z.-H. Cheng, *J. Magn. Magn. Mater.* **303**, 84 (2006).
- [102] J. Kaspar and D. R. Salahub, *Phys. Rev. Lett.* **47**, 54 (1981).
- [103] B. Rellinghaus, J. Kästner, T. Schneider, E. F. Wassermann, and P. Mohn, *Phys. Rev. B* **51**, 2983 (1995).
- [104] R. Huang, Y. Liu, W. Fan, J. Tan, F. Xiao, L. Qian, and L. Li, *J. Am. Chem. Soc.* **135**, 11469 (2013).
- [105] M. Balli, S. Jandl, P. Fournier, and A. Kedous-Lebouc, *Appl. Phys. Rev.* **4**, 021305 (2017).
- [106] V. K. Pecharsky, and K. A. Gschneidner Jr., *Phys. Rev. Lett.* **78**, 4494 (1997).
- [107] O. Tegus, E. Brück, K. H. J. Buschow, and F. R. de Boer, *Nature* **415**, 150 (2002).
- [108] T. Krenke, E. Duman, M. Acet, E. F. Wassermann, X. Moya, Ll. Mañosa, and A. Planes, *Nat. Mater.* **4**, 450 (2005).
- [109] M. P. Annaorazov, K. A. Asatryan, G. Myaligulyev, S. A. Nikitin, A. M. Tishin, and A. L. Tyurin, *Cryogenics* **32**, 867 (1992).
- [110] B. D. Cullity and C. D. Graham, *Introduction to Magnetic Materials*, 2nd ed. (John Wiley & Sons, Inc., New York, 2009).
- [111] M. Kresch, Temperature Dependence of Phonons in Elemental Cubic Metals Studied by Inelastic Scattering of Neutrons and X-Rays, Ph.D. thesis, California Institute of Technology, 2009.
- [112] <http://nrxs.com>.
- [113] W. M. Visscher, *Ann. Phys.* **9**, 194 (1960).
- [114] D. W. Johnson and J. C. H. Spence, *J. Phys. D: Appl. Phys.* **7**, 771 (1974).
- [115] H. J. Lipkin, *Ann. Phys.* **18**, 182 (1962).
- [116] H. J. Lipkin, *Phys. Rev. B* **52**, 10073 (1995).
- [117] M. Y. Hu, *Hyperfine Interact.* **237**, 64 (2016).